Clinical Science (2019) **133** 225–238
https://doi.org/10.1042/CS20180842

PORTLAND PRESS

Research Article

Rare mutations of *ADAM17* from TOFs induce hypertrophy in human embryonic stem cell-derived cardiomyocytes via HB-EGF signaling

Yifang Xie[1,2], Anyun Ma[2], Boshi Wang[2], Rui Peng[2,3], Yingchun Jing[2,4], Deqian Wang[5], Richard H. Finnell[6,7], Bin Qiao[8], Yongming Wang[9,10], Hongyan Wang[1,2,3,11] and Yufang Zheng[2,3,4]

[1]Institutes of Biomedical Sciences, Fudan University, Shanghai 200032, China; [2]Obstetrics and Gynecology Hospital, Institute of Reproduction and Development, State Key Laboratory of Genetic Engineering at School of Life Sciences, Fudan University, Shanghai 200011, China; [3]Key Laboratory of Reproduction Regulation of NPFPC, Collaborative Innovation Center of Genetics and Development, Fudan University, Shanghai 200032, China; [4]Institute of Developmental Biology & Molecular Medicine, Fudan University, Shanghai 200433, China; [5]School of Life Sciences, Fudan University, Shanghai 200438, China; [6]Departments of Molecular and Cellular Biology and Medicine, Baylor College of Medicine, Houston, Texas 77030, USA; [7]Collaborative Innovation Center for Genetics & Development, School of Life Sciences, Fudan University, Shanghai 200438, China; [8]Institute of Cardiovascular Disease, General Hospital of Jinan Military Region, Jinan 250022, China; [9]MOE Key Laboratory of Contemporary Anthropology at School of Life Sciences, Fudan University, Shanghai 200438, China; [10]Zhongshan Hospital of Fudan University,180 Fenglin Road, Shanghai 200032, China; [11]Children's Hospital of Fudan University, 399 Wanyuan Road, Shanghai 201102, China

Correspondence: Yufang Zheng (zhengyf@fudan.edu.cn) or Yongming Wang (ymw@fudan.edu.cn) or Hongyan Wang (wanghy@fudan.edu.cn)

Tetralogy of Fallot (TOF) is the most common cyanotic form of congenital heart defects (CHDs). The right ventricular hypertrophy is associated with the survival rate of patients with repaired TOF. However, very little is known concerning its genetic etiology. Based on mouse model studies, a disintergrin and metalloprotease 10/17 (ADAM10 and ADAM17) are the key enzymes for the NOTCH and ErbB pathways, which are critical pathways for heart development. Mutations in these two genes have not been previously reported in human TOF patients. In this study, we sequenced *ADAM10* and *ADAM17* in a Han Chinese CHD cohort comprised of 80 TOF patients, 286 other CHD patients, and 480 matched healthy controls. Three missense variants of *ADAM17* were only identified in 80 TOF patients, two of which (Y42D and L659P) are novel and not found in the Exome Aggregation Consortium (ExAC) database. Point mutation knock-in (KI) and *ADAM17* knock-out (KO) human embryonic stem cells (hESCs) were generated by CRISPR/Cas9 and programmed to differentiate into cardiomyocytes (CMs). Y42D or L659P KI cells or complete KO cells all developed hypertrophy with disorganized sarcomeres. RNA-seq results showed that phosphatidylinositide 3-kinases/protein kinase B (PI3K/Akt), which is downstream of epidermal growth factor receptor (EGFR) signaling, was affected in both ADAM17 KO and KI hESC-CMs. *In vitro* experiments showed that these two mutations are loss-of-function mutations in shedding heparin-binding EGF-like growth factor (HB-EGF) but not NOTCH signaling. Our results revealed that CM hypertrophy in TOF could be the result of mutations in *ADAM17* which affects HB-EGF/ErbB signaling.

Received: 26 September 2018
Revised: 22 December 2018
Accepted: 03 January 2019

Accepted Manuscript Online: 04 January 2019
Version of Record published: 22 January 2019

Introduction

Tetralogy of Fallot (TOF) is the most common cyanotic congenital heart defect (CHD) in neonatal patients. The prevalence of TOF is about 3 per 10000 live births, and accounts for 7–10% of all congenital cardiac malformations [1,2]. The main features of TOF are pulmonary outflow tract obstruction, ventricular septal defect, overriding aortic root, and right ventricular hypertrophy. Both genetic and environmental factors have been shown to contribute to the prevalence of CHDs [3–6]. However, very limited genetic data is available on TOF due to its high mortality [7].

Clinical Science (2019) **133** 225–238
https://doi.org/10.1042/CS20180842

The NOTCH pathway is a crucial cell-fate regulator for heart development [8] and NOTCH pathway genes have been implicated in the etiology of TOF. For example, there is an association between Alagille syndrome and TOF with mutations in the NOTCH ligand gene *JAGGED1 (JAG1)* [9,10]; and *de novo* copy number variants in loci covering both *NOTCH1* and *JAG1* were identified in sporadic non-syndromic TOF cases [11]. The activation of the NOTCH pathway requires three proteolytic cleavage steps. Within these steps, the action of a disintegrin and metalloprotease 10 and/or 17 (ADAM10 & ADAM17), which cleaves at the extracellular juxtamembrane region of NOTCH1 [12], is the rate-limiting step for NOTCH1 activation [13]. Notably, ADAM10 and ADAM17 also have critical function in the epidermal growth factor (EGF)-ErbB signaling by cleaving EGF ligands, such as heparin-binding EGF-like growth factor (HB-EGF) [14,15]. The ErbB pathway is also critical for heart development [16,17]. The importance of these two genes in heart development are also demonstrated in mouse models as both *Adam17* [18–21] and *Adam10* [22] knock-out (KO) mice have severe defects in cardiac development. Despite these previous biochemical and animal model studies, currently there is no report on *ADAM10* and *ADAM17* mutations in TOF.

Another challenge to studying the causality of human mutations is that it is almost impossible to validate the functional changes in humans. However, recent advances in human embryonic stem cells-derived cardiomyocytes (hESC-CMs) combined with CRISPR/Cas9 genome editing technologies provide powerful tools to analyze the functions of human mutations. This cell-based human model system has its unique advantages in screening the effects of human mutations acquired from sequencing data. This system not only provides a tool to study the molecular and cellular mechanisms involved in normal and abnormal cardiomyocyte (CM) development and maturation, but also allows us to validate previous findings in animal model systems. Therefore, this system is good for exploring the impact of genetic defects on early cardiac development and gain novel insights into the underlying disease mechanisms of CHD [23,24].

Herein, we sequenced both *ADAM10* and *ADAM17* genes in 80 sporadic TOF patients, and compared with 286 other CHD patients and 480 unaffected controls. We identified three *ADAM17* missense mutations in 80 TOF patients, but not in the other 286 CHD or 480 control samples. By using genome-edited hESC-CMs system, we were able to show that the two novel *ADAM17* mutations induced CM hypertrophy. Our results revealed that CM hypertrophy in TOF could be the primary symptom caused by mutations in *ADAM17* affecting HB-EGF but not NOTCH signaling.

Materials and methods

Human subjects

Blood samples from 366 CHD patients (mean age 2.9 $\pm$ 2.6 years, 54.7% male, including 157 VSD [43%], 80 TOF [22%], 74 ASD [20%], and 55 others [15%]) were collected between 2008 and 2013 from the Cardiovascular Disease Institute of Jinan Military Command (Jinan, Shandong, China). Sporadic CHD cases were diagnosed based on echocardiography, with some diagnoses further confirmed surgically. Patients with a positive family history of CHD in a first-degree relative, maternal diabetes mellitus, maternal exposure to teratogens or therapeutic drugs during gestation, were all excluded. All of the CHD cases were classified according to previously described methodology [25]. The 480 controls (mean age 7.1 $\pm$ 3.7 years, 49.8% male) were ethnically and gender-matched unrelated healthy volunteers recruited from the same geographical area. Individuals who manifested additional syndromes or who had a positive family history of CHD in a first-degree relative were also excluded from controls.

These studies were conducted in accordance with the Declaration of Helsinki. Protocols were reviewed and approved by the Ethics Committee of the School of Life Sciences, Fudan University and local ethics committees prior to the commencement of the study. Written informed consent from the parents or guardians of the children was obtained.

Approximately 2 ml of peripheral blood was collected from each test subject. Genomic DNA of each test subject was isolated from blood samples using conventional reagents and was quantified using a NanoDrop2000 (Thermo Scientific).

DNA sequencing and SNaPshot

The genomic structures of *ADAM10* and *ADAM17* (NG_033876.1 and NG_029873.1) were extracted from NCBI. All exons were PCR-amplified from 48 TOF samples and 96 controls and sent for Sanger sequencing using the ABI Prism BigDye system according to the manufacturer's instructions (ABI, Foster City, CA). The primers used for sequencing are listed in Supplementary Tables S1 and S2. Five missense mutations in ADAM17 were identified in these 48 TOF samples but not controls. SNaPshot analysis was used to confirm these five sites in the rest of the 318 cases and 384

controls. The samples for sequencing and genotyping were run on an ABI 3730 automated sequencer and analyzed by SeqMan and Peakscan, respectively.

Cell culture

Human ESCs line H9 (WA09) was obtained from WiCell Research Institute (Madison, WI) and were cultured on Matrigel-coated (Corning 354277) plates in mTeSR1 medium (StemCell Technologies, cat # 05850) with Rock inhibitor (Stem Cell Tech., Y27632). Results for subsequent experiments are based on 1 hESC line (WA09). Human HEK293T cells and monkey COS-7 cells were cultured in DMEM supplemented with 10% FBS. All cells were maintained under conditions of 37 °C, 5% CO_2 and passaged by using 0.5mM EDTA.

Plasmid construction

To construct episomal vector-based CRISPR/Cas9 system (epiCRISPR) plasmid for ADAM17 KO, guide RNA was designed, synthesized, and cloned into BspQI restriction sites of the epiCRISPR plasmid [26] by using primers listed in Supplementary Table S4.

C-flag-tagged human ADAM17 (NM_003183.4) cDNA was purchased from Vigene Biosciences (CH893896) and cloned into pRK5 vector. All mutations of ADAM17 were generated using a QuickChange Sit e-Directed Mutagenesis Kit (Stratagene). All plasmids used in this study were confirmed by DNA sequencing.

CRISPR/Cas9-mediated genome editing

To generate KO hESCs, 2 μg ADAM17-KO plasmid was transfected into a well of a six-well plate using lipofectamine 3000 (Life Technologies). After 24 h, transfected cells were selected with 0.3 μg/ml puromycin. Ten days later, the cells were disassociated into single cells and reseeded onto new Matrigel-coated wells for individual colony picking. Two weeks after reseeding, single colonies were picked. Genomic DNA was extracted and PCR was performed for the targeting site and sent for sequencing.

To generate KI hESCs, sgRNA plasmids were designed, synthesized, and ligated into the px458 plasmid with enhanced specificity SpCas9 (eSpCas9) by using primers listed in Supplementary Table S4. Donor plasmid based on puc57 plasmid was synthesized from Generay Biotech, which includes 5′ and 3′ 750 bp homologram (including exon with point-mutation and adjacent intronic sequences), PGK promoter driving the expression of Puro-TK, and two loxP sites. Both the px458 with targeting sgRNA and the KI donor plasmid were transfected into hESCs using lipofectamine 3000, and transfected cells were selected with puromycin. The recombined cells survived and were genotyped. Finally, the selection cassette was excised by transfection of Cre. After negative selection using ganciclovir, mutated cells were obtained for PCR and confirmed by DNA sequencing.

Cardiac differentiation of human ESCs

Human ES cells were induced to differentiate into CMs according to a previously published protocol [27]. At day 4, ESCs were dissociated with 0.5 mM EDTA into single cells, and then seeded onto Matrigel at 0.5 × 105 cells per cm^2 in mTeSR1 with Rock inhibitor. The mTeSR1 medium was changed every 24 h until cells had grown to 80–90% confluence. At day 0, cells were changed to 4 ml 1640+B27 (without insulin) with 6 uM CHIR99021 (Selleck, Sl263) for 2 days. At day 2, 4 ml 1640+B27 (without insulin) were added. At day 4, 5 uM IWP-2 (sigma 686770-61-6) were added with 4 ml 1640+B27 (without insulin). At day 6, IWP-2 was removed; cells were cultured with 1640+B27 (without insulin) for another 2 days. At day 8, the media was changed to 1640+B27 hereafter. Every 48 h, cells were gently changed with new media. At day 15, CMs were passaged with 0.25% trypsin-EDTA and at day 35, CMs can be used for functional assays and RNAseq.

RNA isolation, cDNA Synthesis, and qPCR

Total RNA from cultured cells was extracted using RNAsimple Total RNA Kit (TIANGEN; DP419), according to the manufacturer's instructions. RNA was reverse transcribed into cDNA with FastQuant RT kit including gDNAase (TIANGEN; KR106-02). For the quantitative detection of mRNA levels, quantitative real-time PCR was performed using SuperReal PreMix Plus-SYBR Green (TIANGEN; FP205-02) on LightCycler96 qPCR system, and GAPDH levels were used to normalize the gene-specific expression levels. Primers used for qPCR are listed in Supplementary Table S3.

Clinical Science (2019) **133** 225–238
https://doi.org/10.1042/CS20180842

Immunofluorescence staining

CMs or COS-7 cells were washed with PBS three times for 5-min each, and fixed with 4% paraformaldehyde for 15 min at room temperature. Cells were permeabilized with 0.2% Triton X-100 in PBS for 15 min and were blocked with 3% BSA in PBS for 1 h at room temperature. Then, samples were incubated at 4 °C overnight with following antibodies diluted at 1:500 in blocking solution: cardiac troponin T (cTnT) (Rabbit monoclonal, Proteintech, 15513-1-AP; a-actinin (Mouse monoclonal, Sigma, A7732; 1:500), flag (9A3, Mouse monoclonal, CST, 8146T). After three washes with PBS for 5-min each, cells were incubated with appropriate Alexa fluorogenic secondary antibodies (Alexa Fluor 568, Abacam, ab175473, 1:500) (Alexa Fluor 488, Abacam, ab150077, 1:500) at room temperature for 1 h followed by 15 min of DAPI staining for nuclei visualization. At least four random fields were selected during cell counting to reduce bias.

Calcium imaging traces using Fluo-4 AM

CMs were dissociated and seeded into Matrigel-coated glass bottom cell culture dishes (Nest, 801001). Then cell were added with 4 μM Fluo-4 AM in Tyrode's solution for 30 min at 37 °C. Finally, cells were washed with Tyrode's solution three times before being imaged using a confocal microscope with a 63× lens. Videos of spontaneous Ca^{2+} transients were taken at 20 fps for 10 s recording durations. Ca^{2+} responses were quantified using ImageJ to average the measure intensity of Ca^{2+} regulation. Specific regions of spontaneously contracting microclusters were selected and the peak amplitude of the calcium transient expressed relative to the baseline fluorescence measured between action potentials (F/F0) was quantified using ImageJ.

Western blots

Cells were washed with cold PBS, and lysed in cold lysis buffer (150 mM NaCl, 50mM Tris-Cl, pH 7.4, 1 mM EDTA, 1% Triton, complete mini tablet-protease inhibitor cocktail tablets [Roche]). The proteins were separated by 10% SDS–PAGE and transferred to PVDF membranes. After blocking with 5% BSA in TBS with Tween (TBST), the membrane was incubated overnight at 4°C with one of the following primary antibodies: GADPH (CST, 5174S), flag (9A3, Mouse monoclonal, CST, 8146T), ADAM17 (Abcam, ab13535), and GFP (Abcam, ab1218). Next day, the membrane was washed with TBST for three times, and incubated with corresponding anti-mouse/rabbit/goat secondary antibodies (mouse, Abcam, ab6728) (rabbit, Abcam, ab6721) (goat, Abcam, ab6789) at 1:10000 dilution at room temperature for 1 h. Signal intensity was quantified with ImageJ software.

RNA-seq and transcriptome analysis

RNA-seq was carried out by Shanghai Biotechnology Corporation (SBC). In brief, three colonies of cells of each genotype were sent for RNA-seq analysis. Total RNA was isolated using TRIZOL Reagent (Invitrogen) following the provider's instructions. The cDNA library was constructed using TruSeq RNA Sample Prep Kit and then sequenced on an Illumina HiSeq 2000 system (Illumina, Inc.). Sequencing raw reads were preprocessed by filtering out rRNA reads, sequencing adapters, short-fragment reads, and other low-quality reads. Hisat2 (version: 2.0.4) [28] was used to map the cleaned reads to the human hg38 reference genome with two mismatches. After genome mapping, Stringtie (version:1.3.0) [29,30] was run with a reference annotation to generate fragments per kilobase million (FPKM) values for known gene models. The sample correlation was shown in Supplementary Figure S3. Differentially expressed genes were identified using edger [31]. The p-value significance threshold in multiple tests was set by the false discovery rate (FDR) [29,32,33]. The fold-changes were also estimated according to the FPKM in each sample. The differentially expressed genes were selected using the following filter criteria: FDR P-value ≤ 0.05 and fold-change ≥ 2. Kyoto Encyclopedia of Genes and Genomes (KEGG) enrichment and classification, biological processes in Gene Ontology (GO) were analyzed for differentially expressed genes.

Transfection and ectodomain shedding assays

Alkaline phosphatase (AP)-tagged HB-EGF plasmid was a gift from Dr Shigeki Higashiyama (Department of Biochemsitry and Molecular Genetics, Ehime University School of Medicine, Shitsukawa, Toon, Japan). ADAM17$^{-/-}$ 293T cells [34] were grown to 60% confluency and then transfected with AP-HB-EGF plasmid together with wild-type (WT) or mutant ADAM17 using Lipofectamine 2000 (Invitrogen, Grand Island, NY). When the cells were confluent, they were washed in Opti-MEM (Gibco, Grand Island, NY) for 1 h. Fresh Opti-MEM with or without 25 ng/ml phorbol-12-myristate-13-acetate (PMA) was added for 1 h to stimulate shedding as described before [14,15]. After incubating with the AP substrate 4-nitrophenyl phosphate (4-NPP), the AP activities in the supernatant were measured at 405 nm. Three identical wells were prepared, and the ratio of AP activity in the supernatant was calculated

Table 1 Missense mutations of *ADAM17* and *ADAM10* detected in our CHD cohort

Mutation location	cDNA change	a.a. change	AF in cases[1]	AF in TOFs[2]	AF in controls[3]	AF in ExAC
ADAM17 exon2	c.124 T>A	Y42D	0|1 (366) = 0.0014	0|1 (80) = 0.0063	0|0 (480) = 0	0
ADAM17 exon5	c.536 A>G	Q179R	0|1 (366) = 0.0014	0|1 (80) = 0.0063	0|4 (480) = 0.0042	9.08e-05
ADAM17 exon16	c.1976T>C	L659P	0|1 (366) = 0.0014	0|1 (80) = 0.0063	0|0 (480) = 0	0
ADAM17 exon19	c.2243C>T	A748V	0|1 (366) = 0.0014	0|1 (80) = 0.0063	0|0 (480) = 0	0.001542
ADAM10 exon7	c.763A>G	T255A	3|6 (366) = 0.016	0|1 (80) = 0.0063	1|8 (480) = 0.010	0.0007415

[1]The numbers are the homo|het carriers in (tested) CHD cases.
[2]The numbers are the homo|het carriers in (tested) TOF cases.
[3]The numbers are the homo|het carriers in (tested) controls.

by values from the second hour divided by values from the first hour. Each experiment was conducted at least three times. Student's *t* test for paired samples was used to determine statistical significance. Differences were considered statistically significant at $P<0.05$.

Dual-luciferase reporter assay

Dual-luciferase assays were performed using the Dual-Luciferase Assay system from Promega. ADAM17$^{-/-}$ 293T cells were seeded in 24-well culture plates and grown to 70–80% confluency. The cells from each well were transfected with 400 ng ADAM17 WT or MUT or empty vector plasmids, 100 ng of CSL (CBF1/RBP-Jκ) luciferase reporter, and internal control 10 ng of Renilla-luciferase plasmid, using Lipofectamine 2000 (Invitrogen). After 48 h, the cells were lysed and assayed for luciferase activity. Luciferase activity was corrected for transfection efficiency. Student's *t* test for paired samples was used to determine statistical significance. Differences were considered statistically significant at $P<0.05$.

Results

Novel missense variants of *ADAM17* detected in TOF patients

A total of 80 sporadic TOF patients, 286 other CHD patients, and 480 matched healthy controls were collected during 2008–2013 as described in the Materials and methods section. Target sequencing on all exons of *ADAM10* and *ADAM17* were performed in TOF patients first. Only four missense single nucleotide variants (SNVs) of *ADAM17* and one missense SNV of *ADAM10* were identified in 80 TOF patients (Table 1). When the other 286 CHD or 480 control samples were further sequenced, only three *ADAM17* mutations were detected in TOF patients (c.124 T>A, c.1976T>C, c.2243C>T), which were verified by Sanger sequencing (Suplementary Figure S1). Two of the *ADAM17* mutations (c.124 T>A p.Y42D and c.1976T>C p.L659P) are novel, based on our control sample and the Exome Aggregation Consortium (ExAC) database [35] (Table 1).

ADAM17 knock-in and KO did not affect pluripotency of hESCs

Previous studies showed that coding variants which are predicted to affect protein function are more likely to be causal [36,37]. To study the function of these mutations, we used hESCs-derived CMs to test the impact of these case-specific ADAM17 mutations on protein function.

The first step is to generate genome-edited hESC lines carrying different ADAM17 mutations. Using CRISPR/Cas9 and cre-loxp-based genome editing strategy (Figure 1A), we generated three *ADAM17* heterozygote knock-in (KI) (T124A, T1976C, and C2243T) hESC lines and the mutations were confirmed by Sanger sequencing (Figure 1B–D). The newly developed SpCas9 (eSpCas9) was used in our experiments to reduce off-target effect and enhance specificity [38]. We also generated *ADAM17* KO hESCs with a 4 bp deletion compared with WT cells (Figure 1E,F) using the epiCRISPR system which we previously developed [26]. Luckily, the KO hESCs were homozygotes and the complete loss of ADAM17 protein was confirmed by Western blot in two different single cell colonies (Figure 1G).

We subsequently examined whether these edited cell lines could maintain pluripotent characteristics by checking their morphologies and expression of pluripotency markers. Similar to WT hESCs, all three mutated hESCs (Y42D, L659P, A748V corresponding to T124A, T1976C, C2243T) had normal morphologies and stained positive for pluripotency markers OCT4 and Tra1-60 (Figure 1H). Therefore, neither knocking-in nor knocking-out of *ADAM17* affected the pluripotency of hESCs.

Clinical Science (2019) **133** 225–238
https://doi.org/10.1042/CS20180842

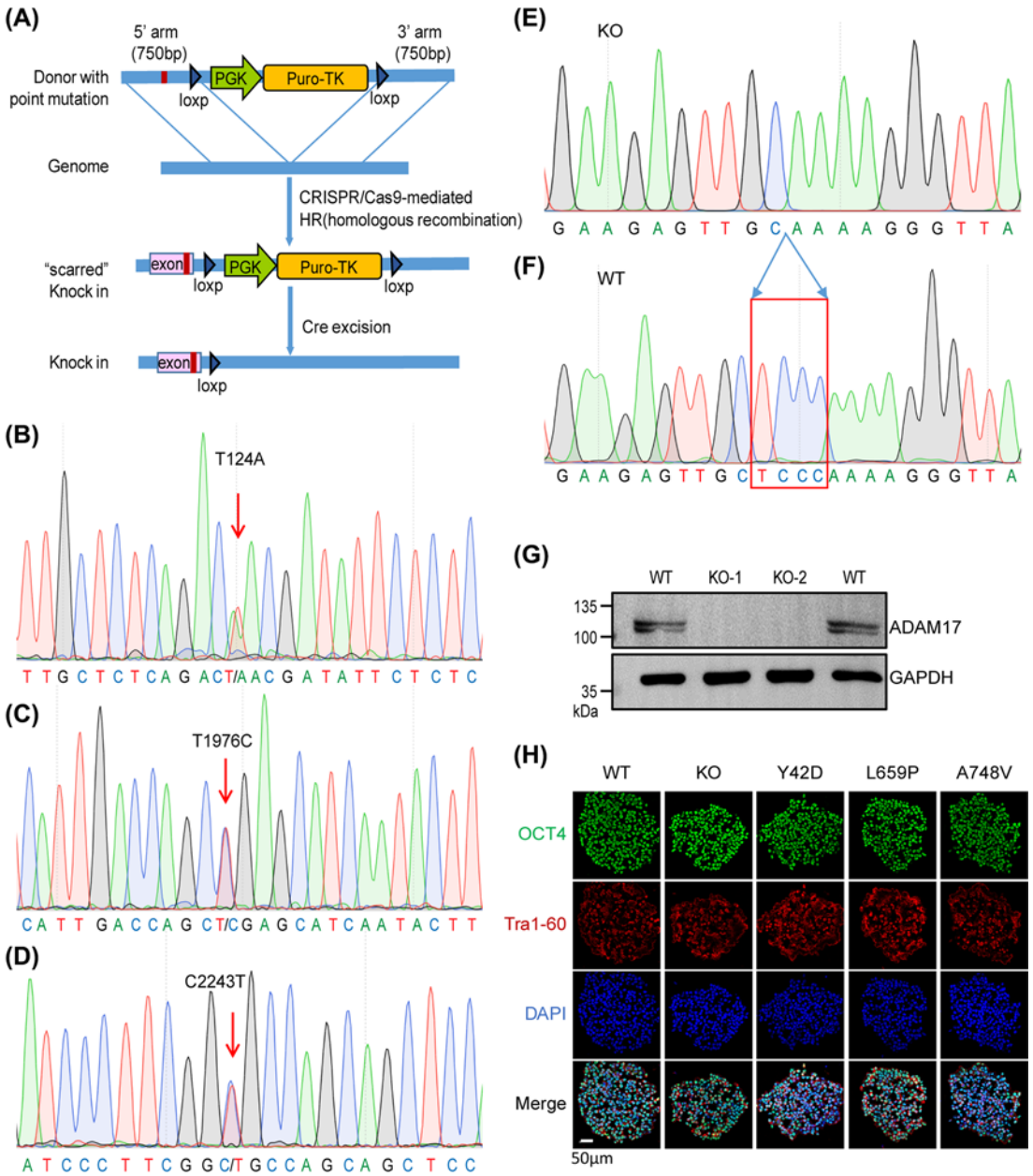

Figure 1. Generating genome-edited hESCs by CRISPR/Cas9 system

(**A**) The overview of genome editing system for KI. The sequencing confirmation of T124A (**B**); T1976C (**C**); C2243T (**D**); KI hESCs and KO (**E**); and WT (**F**) hESCs. All KI hESCs are heterozygous and KO is homozygous. (**G**) Two colonies each of WT and KO hESCs were subjected to Western blotting for ADAM17. GAPDH was used as loading control. (**H**) Immunofluorescent staining of WT, KO, Y42D (T124A), L659P (T1976C), and A748V (C2243T) hESCs with pluripotency marker octamer-binding transcription factor 4 (OCT4) (green) and Tra1-60 (red). DAPI was used for nucleus staining (blue) (*N*=4).

ADAM17 KI and KO hESC-CMs were hypertrophic

The hESC lines were induced to differentiate into CMs using a previously published monolayer stepwise differentiation protocol (Figure 2A) [27]. Eight to ten days after the induction of differentiation, spontaneously beating cells were observed. At day 15, beating CMs were dissociated and seeded into Matrigel-coated plates for further analysis. These CMs exhibited positive staining for sarcomeric proteins such as α-actinin and cardiac troponin T (Figure 2B). Markedly, significant hypertrophy was observed in *ADAM17* KO and Y42D and L659P mutant hESC-CMs, but not

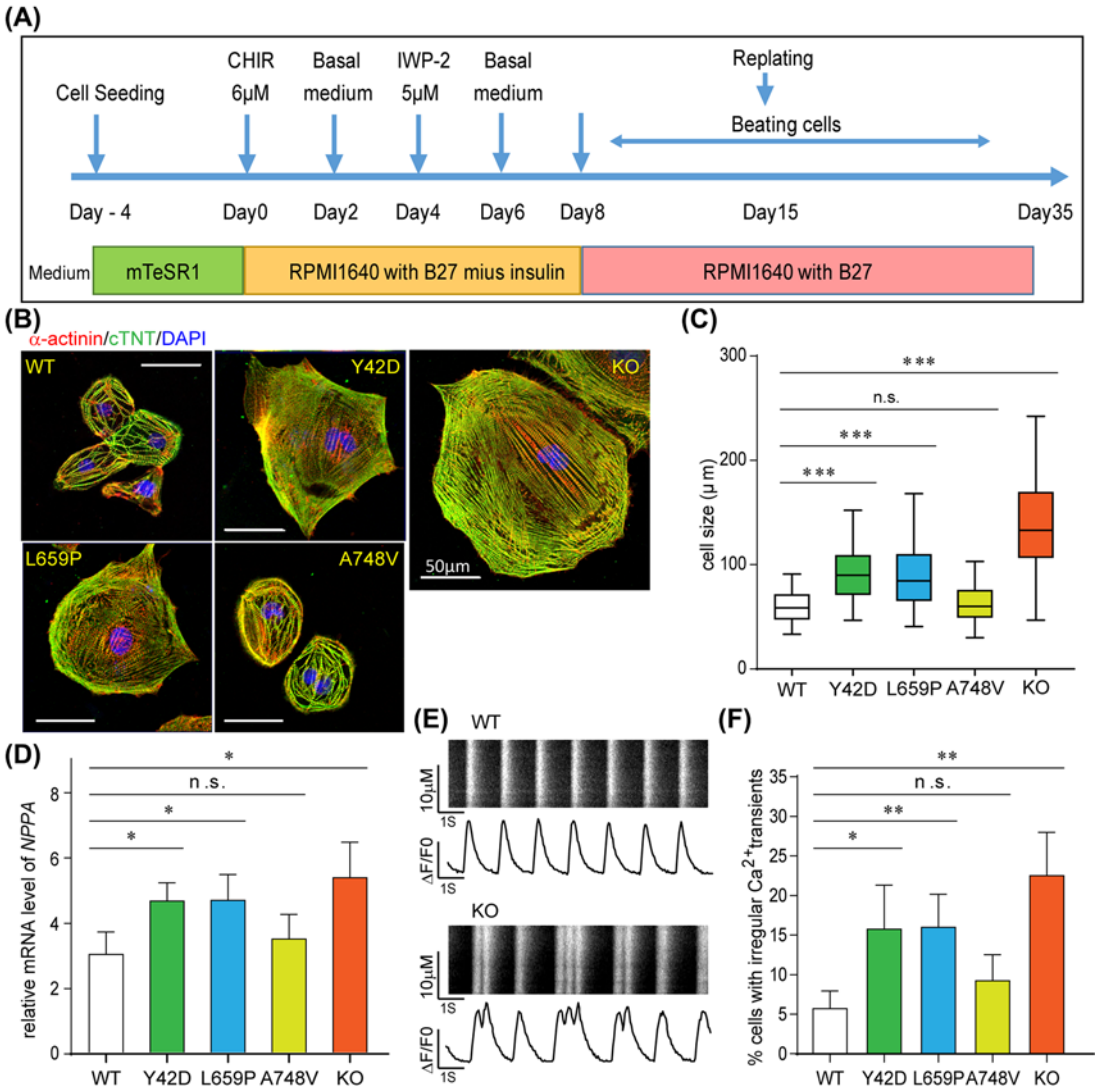

Figure 2. ADAM17 KO, Y42D and L659P KI hESC-CMs are hypertrophy with irregular calcium transient signal

(**A**) An illustration of the stepwise differentiation protocol for hESC-CMs. (**B**) Immunofluorescent staining of WT, KO, Y42D, L659P, and A748V hESC-CMs with CM markers α-actinin (red) and cTnT (green). DAPI was used for nucleus staining (blue). (**C**) The box plot of cell sizes for five different hESC-CMs (n=60 for each line). (**D**) The expression levels of cardiac hypertrophy marker *NPPA* were quantified by qPCR in hESC-CMs (N=4). (**E and F**) The Ca^{2+} transient signals in these hECS-CMs. The representative regular signals in WT and irregular signals in KO cells were shown in (E). (F) N=4 and over 60 cells were randomly selected each time and percentages of cells with irregular Ca2+ transient were calculated. Data are presented as mean ± S.E.M. Student's t test for paired samples was used to determine statistical significance. $^{*}P<0.05$, $^{**}P<0.01$, and $^{***}P<0.001$.

in the A748V mutant hESC-CMs (Figure 2B), which was also reflected in the cell sizes (Figure 2C). We also examined the expression levels of *NPPA*, a CM hypertrophy marker [39] (Figure 2D), which was significantly higher in *ADAM17* KO and Y42D and L659P mutant hESC-CMs but not A748V mutant hESC-CMs. In addition, *ADAM17* KO and Y42D and L659P mutant hESC-CMs also have disorganized sarcomeres (Supplementary Figure S2). The normal hESC-CMs displayed regular spontaneous rhythmic calcium cycling while the hypertrophic hESC-CMs displayed irregular rhythms (Supplementary Videos S1 and S2). This is also further confirmed by intracellular calcium signaling with the fluorescent Ca^{2+} dye Fluo-4 AM. Compared with WT and ADAM17 A748V hESC-CMs, the ADAM17 KO, Y42D and L659P mutant hESC-CMs showed significantly more Ca^{2+} transient irregularities (Figure 2E,F).

Clinical Science (2019) **133** 225–238
https://doi.org/10.1042/CS20180842

Phosphatidylinositide 3-kinases/protein kinase B (PI3K/Akt) signaling was altered in mutated hESC-CMs and ADAM17 Y42D and L659P mutants lost HB-EGF shedding

To better understand the molecular and cellular effects of these mutants, the WT, KO, Y42D, L659P, and A748V hESC-CMs were sent for RNA-seq analysis. The RNA-seq results showed that A748V hESC-CMs were very similar to WT hESC-CMs, while KO, Y42D, and L659P hESC-CMs had significant number of differentially expressed genes compared with WT hESC-CMs (Figure 3A). The KEGG enrichment analysis revealed that there were multiple CM-related pathways affected (P-value <0.05) in three hypertrophic CMs, including hypertrophic cardiomyopathy and dilated cardiomyopathy (Figure 3B and Supplementary Table S5). The KEGG classification of the differential genes showed the most affected class in hypertrophic CMs was signal transduction (Supplementary Figure S4). Interestingly, the most affected pathways in three hypertrophic CMs were the phosphatidylinositide 3-kinases/protein kinase B (PI3K/Akt), calcium, and MAPK signaling pathways (Figure 3C, Supplementary Figure S4, and Supplementary Table S6). As both PI3K/Akt and MAPK pathways are downstream of ErbB signaling, these results suggested that probably ErbB signaling, not NOTCH signaling, was affected in the hypertrophic CMs.

To further explore the signaling events during CM differentiation, we performed q-PCR on a set of genes at various time points of WT hESCs differentiation (Figure 4). The set of genes included multiple stage markers and molecules in the NOTCH and ErbB signaling pathways. Two ErbB signaling ligands HB-EGF and transforming growth factor α (TGF-α), which are cleaved by ADAM17 [14], were tested. Our results showed that the expression of stage specific genes correlated well with the differentiation stages, such as *OCT4* for stem cells, *T* and mix paired-like homeobox *(MIXL1)* for mesoderm, NK2 homeobox 5 *(NKX2-5)* for cardiac progenitor cells, and *α-actinin* for CMs. Although the key NOTCH signaling molecules (including ligand *JAG-1*, receptor *NOTCH1*, S2 enzyme *ADAM10*, and downstream target hes family bHLH transcription factor 1 [*HES1*]) were all up-regulated at mesoderm to cardiac progenitor stages (days 2–6), they were slightly down-regulated at CM stage (day 8–12). Instead, both *ADAM17* and *HB-EGF* were constantly up-regulated at the CM stage (day 8–12), while TGF-α was up-regulated only at the mesoderm stage and then sharply down-regulated at the CM stages (Figure 4).

To further explore the effects of *ADAM17* mutations in HB-EGF shedding and NOTCH signaling, *in vitro* assays were carried out. *ADAM17*-KO 293T cells were transfected with different ADAM17 expressing plasmids and AP-tagged HB-EGF plasmid. PMA-induced shedding of HB-EGF was examined as previously described [14,20]. Compared with WT ADAM17, only Y42D and L659P mutants lost PMA-induced HB-EGF shedding in *ADAM17*-KO 293T cells (Figure 5A). When exogenous HB-EGF (10 ng/ml) was added to ADAM17 KO, Y42D, and L659P KI hESC-CMs from day 12 to 30. HB-EGF could reduce the cell size of ADAM17 KO hESC-CMs (Supplementary Figure S5). The effects of ADAM17 mutations on NOTCH signaling were further examined by the NOTCH reporter genes CSL luciferase system as well as the expression of the endogenous NOTCH target genes *HES1* and *HEY1*. *ADAM17*-KO 293T cells were transfected with different ADAM17 expressing plasmids and CSL luciferase reporters. The results showed that the impact of the mutations were similar to that of WT ADAM17 on NOTCH signaling (Figure 5B). The expression levels of *HES1* and *HEY1* were examined by q-PCR in 293T cells which were transfected with either WT or mutant ADAM17 expressing plasmids. The results also showed that the ADAM17 mutants do not affect NOTCH signaling (Figure 5C,D). Immunofluorescent experiments showed that none of the mutations affected the membrane location of ADAM17 in COS-7 cells (Figure 5E). However, Y42D mutation down-regulated the expression level of ADAM17 in *ADAM17*-KO 293T cells (Figure 5F), which can be blocked by proteasome inhibitor MG132 (Figure 5G).

Taken together, ADAM17 Y42D significantly decreased the protein expression level of ADAM17, while the Y42D and L659P mutations strongly inhibited the ADAM17-dependent shedding of HB-EGF, yet had no effect on NOTCH signaling.

Discussion

Although recent whole exome sequencing studies on large CHD cohorts confirmed the importance of rare variants in the etiology of CHDs [40–44], just how these variants contribute to the pathology and phenotypes of CHDs remains unclear. By using a hESC-CMs model, we were able to demonstrate that two novel variants of *ADAM17* identified in TOF patients can induce CM hypertrophy. The right ventricle hypertrophy of TOF is considered as a secondary symptom due to pulmonary outflow tract obstruction. But our study suggested that the right ventricle hypertrophy could also be a primary symptom of TOF due to the genetic background of the infant. Even after surgical repair, the right ventricular hypertrophy is risk factor for sudden death in patients with surgically repaired TOF [45]. Therefore, the primary phenotype may affect the outcome of these patients after TOF repair surgery.

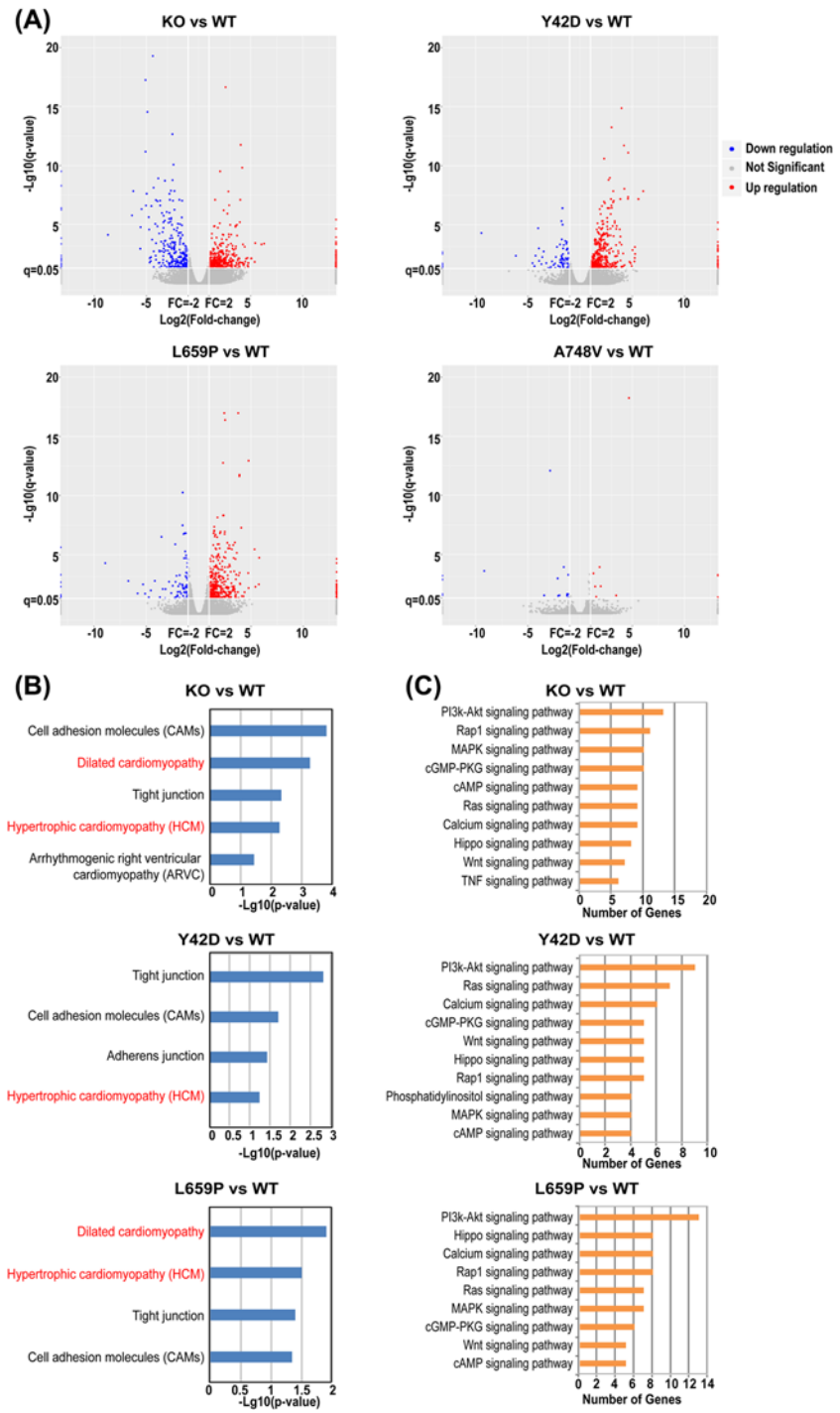

Figure 3. The RNA-seq results of ADAM17 KO, Y42D, and L659P KI hESC-CMs

(**A**) Volcano maps for differentially expressed genes in KO and KI mutant hESC-CMs compared with WT hESC-CMs. The differential genes were analyzed for KEGG pathway and classification enrichment. CMs-related KEGG pathways (*P*-value <0.05) were shown in (**B**)**.** The hypertrophic cadiomyopathy (HCM) pathway in Y42D vs WT group was also included in (B) with a *P*-value $=0.057$. The signaling pathways with most differential genes within signal transduction were shown in (**C**).

Clinical Science (2019) **133** 225–238
https://doi.org/10.1042/CS20180842

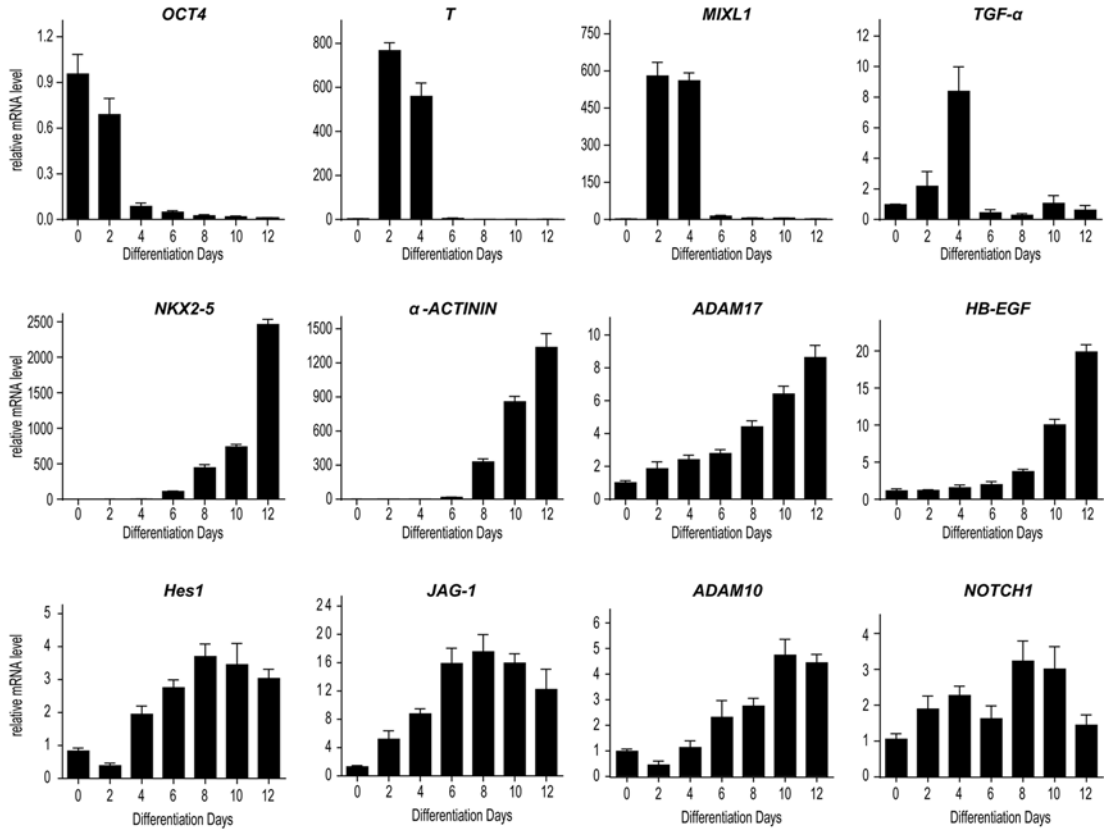

Figure 4. The q-PCR results of different genes during hESCs differentiation

WT hESCs were collected at days 0, 2, 4, 6, 8, 10, and 12. Total RNAs were extracted and subjected to q-PCR for different genes. GAPDH was used as internal control and the relative mRNA levels were calculated (*N*=3).

There are three case-specific ADAM17 missense mutations identified within our cohort. However, based on the ExAC database, which contains genomic data on a control population of over 60000 individuals, the A748V mutation is a rare variant. Not only did this variant fail to affect ADAM17 function, but the A748V-KI hESC-CMs also differentiated normally. Therefore, genetic screening on causative variants could benefit largely from a large control database such as ExAC, even with a relatively limited patient study cohort.

Although we initiated our screening on ADAM10 and ADAM17 as they are both able to cleave NOTCH1 [13,46,47], we failed to identify any case-specific variants in *ADAM10*. One possibility is that a functional mutation of ADAM10 results in early lethality of the fetus, thus, such a mutation could not be detected in any surviving patients. This is consistent with the data observed in the *Adam10* KO mice [22], as well as KOs for *Notch1* [48] and its downstream targets *Hey1* and *Hey2* [49], all of which died around E9.5–10.5 due to failure of early heart development. On the other hand, *Adam17* KO mice died during the perinatal stage [50] with cardiovascular and lung defects [18,21,51]. Interestingly, both ADAM17 KO and the two hypertrophic mutations, ADAM17 Y42D and L659P, lost HB-EGF shedding. When exogenous HB-EGF was added to early differentiated hESC-CMs, it could rescue the hypertrophy phenotype of ADAM17 KO CMs (Supplementary Figure S5). This further supports the importance of ADAM17-mediated HB-EGF shedding for CMs development. These are the first human data and they are consistent with the previous-reported studies using mouse models, which indicated that ADAM17-mediated HB-EGF shedding is critical for heart development [17,18,20,21]. The cell sizes of ADAM17 Y42D and L659P CMs tended to be smaller, but the statistical results were not significant (Supplementary Figure S5). One possibility is that HB-EGF is needed earlier than day 12 for these two cell lines. The other possibility is that these two different point mutations deregulate additional functions during CM differentiation, which need to be further investigated. We note that one human case was reported in 2011 with a loss-of-function mutation in *ADAM17*. The patient had severe inflammatory skin and bowel diseases in addition to ventricular dilation of heart [52]. As our TOF patients do not have symptoms other than cardiac defects, ADAM17-dependent HB-EGF shedding and Y42D and L659P mutations are likely contributing to

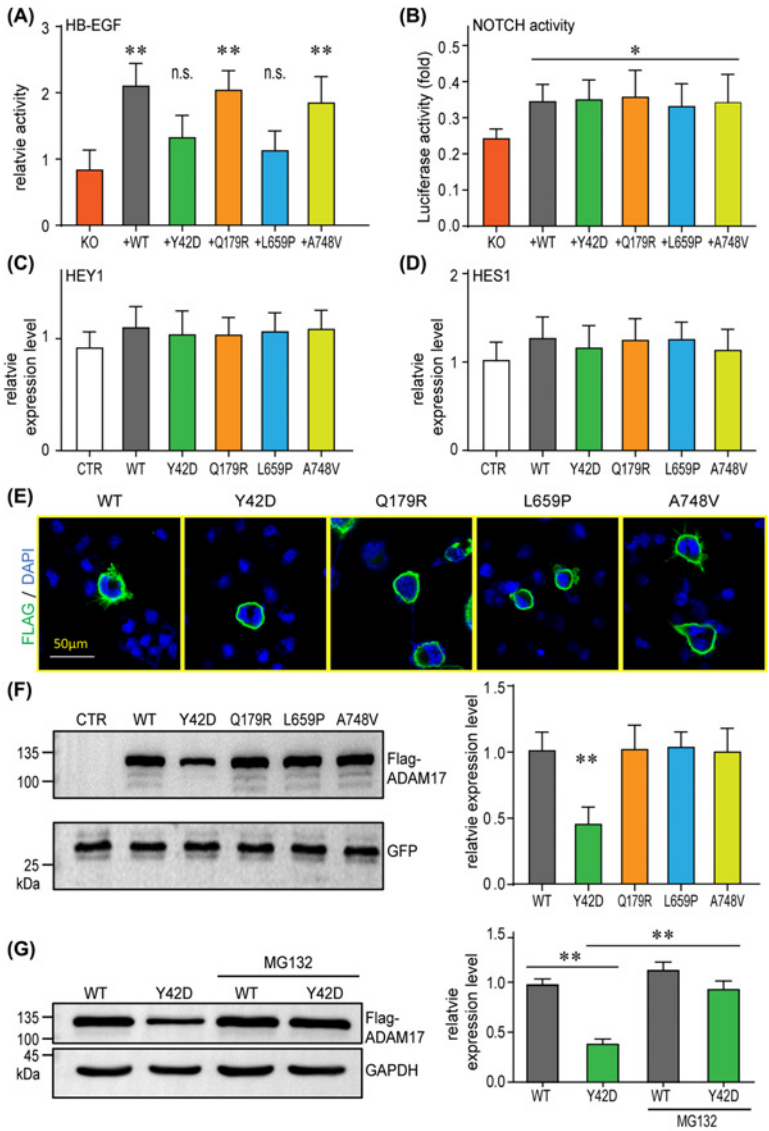

Figure 5. The expression and shedding activity of ADAM17 mutants

(**A**) WT or mutant ADAM17 expression plasmids and substrate AP-tagged HB-EGF plasmids were transfected into *ADAM17*-KO 293T cells and subjected for shedding assay. Supernatants prior to and after PMA stimulation were collected and incubated with 4-NPP for 2 h. OD values were measured at 405 nm. The relative activity was calculated with OD (+PMA)/OD (control) (N=4). (**B**) Dual-luciferase reporter assay for NOTCH activity. *ADAM17*-KO 293T cells were transfected with CSL luciferase reporters with either WT or mutant ADAM17 expression plasmids and subjected to luciferase assay. The relative NOTCH activity was calculated based on the internal control Renilla activity (N=4). (**C,D**) Human 293T cells were transfected with control vector (CTR), WT or mutant ADAM17 expression plasmids, and subjected for q-PCR for NOTCH downstream target genes *HEY1* or *HES1* (N=4). (**E**) C-terminal flag-tagged WT or mutant ADAM17 expression plasmids were transfected into COS-7 cells. Cells were permeabilized with 0.2% Triton X-100 in PBS for 15 min and subjected to immunofluorescent staining with anti-flag antibody and confocal imaging. C-flag-tagged WT and mutant ADAM17 proteins were all located at the cell membrane (green). DAPI (blue) was used for nucleus staining (N=4). (**F**) Human 293T cells were transfected with either WT or mutant ADAM17 expression plasmids and subjected to Western blot with anti-flag antibody. A GFP expression plasmid was co-transfected in all cells and used as loading control. A representative blot was shown on the left and the quantification was shown on the right panel (N=4). (**G**) Human 293T cells were transfected with either WT or ADAM17 Y42D mutant expression plasmids. After 12 h recovery, cells were treated with proteasome inhibitor MG132 (10 μM) for another 12 h. Then cells were lysed and subjected to Western blot with anti-flag antibody. GAPDH was used as loading control. A representative blot was shown on the left and the quantification was shown on the right panel (N=4). In (**A–D, F,G**), data are presented as mean ± S.E.M. and Student's t test for paired samples was used to determine statistical significance. $^{*}P<0.05$ and $^{**}P<0.01$.

Clinical Science (2019) **133** 225–238
https://doi.org/10.1042/CS20180842

the right ventricular hypertrophy of the carrier TOF patients, while the functions of other ADM17-dependent substrates, such as TNF-α, may be important for inflammation in skin and gut. As it has been shown that iRhom2 can regulate substrate selectivity of ADAM17 [53], it will be important to determine how the interaction of iRhom2 with ADAM17 is regulated at Y42 and L659 sites in the developing heart.

Taken together, our study demonstrated that genome-edited hESCs-CMs are a good model system to study the etiology of rare mutations, particular for those involved in the CM maturation process. Using this model, we screened two loss-of-function mutations of ADAM17 which demonstrated that CM hypertrophy in TOF patients may represent the primary phenotype induced by *ADAM17* mutations by affecting HB-EGF signaling. However, as the patients from our cohort are still relatively young, it is too early to ascertain the ultimate health consequences of these patients post-TOF repair surgery. It will take additional surveillance of these patients to determine whether these mutations will affect their right ventricle after they reach adulthood. As there are more and more CHD patients surviving cardiac surgeries, it would be interesting to investigate the long term effects of the correlated genetic mutations in the future.

Clinical perspectives

- Tetralogy of Fallot (TOF) is the most common cyanotic form of congenital heart defects (CHDs). The right ventricular hypertrophy is associated with the survival rate of patients with repaired TOF. However, very little is known concerning its genetic etiology.
- Here we identified two novel *ADAM17* mutations (Y42D and L659P) in TOF patients, which could cause hypertrophy of human embryonic stem cells derived cardiomyocytes when knocked-in as heterozygote by affecting heparin-binding epidermal growth factor-like growth factor/ErbB signaling.
- The right ventricular hypertrophy could be primary phenotype caused by genetic mutations and long term effects of these mutations should be monitored in CHD patients surviving cardiac surgeries.

Acknowledgments
The authors thank the families for their participation in this study.

Competing Interests
The authors declare that there are no competing interests associated with the manuscript.

Funding
This work was supported by grants from the National Natural Science Foundation of China [81741048 and 81870894 (to Y.Z.); 81430005, 31771669, and 31521003 (to H.W.); 81870199 and 31521003 (to Y.W.)]; the National Key Research and Development Program [2016YFC1000502 (to H.W.)]; the Basic Research Project of "Innovation Action Plan" from Shanghai Science and Technology Commission Shanghai Municipality [17JC1400902 (to H.W. and Y.Z.)]; and the National Basic Research Program of China [2015CB943300 (to Y.W.)]. Dr Finnell was supported by a Changjiang Professorship.

Author Contribution
The authors' responsibilities were as follows: Y.Z. conceived and designed the study. Y.X., A.M., Y.J., and D.W. performed experiments on cells. B.Q. collected CHD samples. B.W. and R.P. performed sequencing analysis. Y.W. provided the CRISPR/Cas9 and hESCs culturing systems. Y.Z. and Y.X. performed data analysis. Y.Z. and Y.X. wrote the manuscript. R.F. and Y.W. edited the manuscript. H.W. provided financial support. All authors reviewed/edited the manuscript and approved the final version.

Abbreviations
ADAM10/17, A disintergrin and metalloprotease 10/17; ASD, atrial septal defect; AP, alkaline phosphatase; CHD, congenital heart defect; CMs, cardiomyocytes; cTnT, cardiac troponin T; EGF, epidermal growth factor; EGFR, epidermal growth factor receptor; epiCRISPR, episomal vector-based CRISPR/Cas9 system; eSpCas9, enhanced specificity SpCas9; ExAC, Exome Aggregation Consortium; FPKM, fragments per kilobase million; HB-EGF, heparin-binding EGF-like growth factor; HES1, hes family bHLH transcription factor 1; hESCs, human embryonic stem cells; hESC-CMs, human embryonic stem cells-derived

cardiomyocytes; HEY1, hes-related family bHLH transcription factor with YRPW motif 1; JAG1, Jagged1; KEGG, Kyoto Encyclopedia of Genes and Genomes; KI, knock-in; KO, knock-out; MIXL1, Mix paired-like homeobox; NKX2-5, NK2 homeobox 5; OCT4, octamer-binding transcription factor 4; PI3K/Akt, phosphatidylinositide 3-kinases/protein kinase B; PMA, phorbol-12-myristate-13-acetate; SNV, single nucleotide variant; TNF, tumor necrosis factor; TOF, Tetralogy of Fallot; TGF-α, transforming growth factor α; VSD, ventricular septal defect.

References

1 Starr, J.P. (2010) Tetralogy of fallot: yesterday and today. *World J. Surg.* **34**, 658–668, https://doi.org/10.1007/s00268-009-0296-8
2 Bailliard, F. and Anderson, R.H. (2009) Tetralogy of Fallot. *Orphanet J. Rare Dis.* **4**, 2, https://doi.org/10.1186/1750-1172-4-2
3 Fahed, A.C., Gelb, B.D., Seidman, J.G. and Seidman, C.E. (2013) Genetics of congenital heart disease: the glass half empty. *Circ. Res.* **112**, 707–720, https://doi.org/10.1161/CIRCRESAHA.112.300853
4 Pierpont, M.E., Basson, C.T., Benson, Jr, D.W., Gelb, B.D., Giglia, T.M., Goldmuntz, E. et al. (2007) Genetic basis for congenital heart defects: current knowledge: a scientific statement from the American Heart Association Congenital Cardiac Defects Committee, Council on Cardiovascular Disease in the Young: endorsed by the American Academy of Pediatrics. *Circulation* **115**, 3015–3038, https://doi.org/10.1161/CIRCULATIONAHA.106.183056
5 Jenkins, K.J., Correa, A., Feinstein, J.A., Botto, L., Britt, A.E., Daniels, S.R. et al. (2007) Noninherited risk factors and congenital cardiovascular defects: current knowledge: a scientific statement from the American Heart Association Council on Cardiovascular Disease in the Young: endorsed by the American Academy of Pediatrics. *Circulation* **115**, 2995–3014, https://doi.org/10.1161/CIRCULATIONAHA.106.183216
6 Czeizel, A.E., Dudas, I., Vereczkey, A. and Banhidy, F. (2013) Folate deficiency and folic acid supplementation: the prevention of neural-tube defects and congenital heart defects. *Nutrients* **5**, 4760–4775, https://doi.org/10.3390/nu5114760
7 Morgenthau, A. and Frishman, W.H. (2018) Genetic origins of tetralogy of fallot. *Cardiol. Rev.* **26**, 86–92
8 de la Pompa, J.L. and Epstein, J.A. (2012) Coordinating tissue interactions: Notch signaling in cardiac development and disease. *Dev. Cell* **22**, 244–254, https://doi.org/10.1016/j.devcel.2012.01.014
9 Li, L., Krantz, I.D., Deng, Y., Genin, A., Banta, A.B., Collins, C.C. et al. (1997) Alagille syndrome is caused by mutations in human Jagged1, which encodes a ligand for Notch1. *Nat. Genet.* **16**, 243–251, https://doi.org/10.1038/ng0797-243
10 Oda, T., Elkahloun, A.G., Pike, B.L., Okajima, K., Krantz, I.D., Genin, A. et al. (1997) Mutations in the human Jagged1 gene are responsible for Alagille syndrome. *Nat. Genet.* **16**, 235–242, https://doi.org/10.1038/ng0797-235
11 Greenway, S.C., Pereira, A.C., Lin, J.C., DePalma, S.R., Israel, S.J., Mesquita, S.M. et al. (2009) De novo copy number variants identify new genes and loci in isolated sporadic tetralogy of Fallot. *Nat. Genet.* **41**, 931–935, https://doi.org/10.1038/ng.415
12 Bray, S.J. (2006) Notch signalling: a simple pathway becomes complex. *Nat. Rev. Mol. Cell Biol.* **7**, 678–689, https://doi.org/10.1038/nrm2009
13 van Tetering, G., van Diest, P., Verlaan, I., van der Wall, E., Kopan, R. and Vooijs, M. (2009) Metalloprotease ADAM10 is required for Notch1 site 2 cleavage. *J. Biol. Chem.* **284**, 31018–31027, https://doi.org/10.1074/jbc.M109.006775
14 Sahin, U., Weskamp, G., Kelly, K., Zhou, H.M., Higashiyama, S., Peschon, J. et al. (2004) Distinct roles for ADAM10 and ADAM17 in ectodomain shedding of six EGFR ligands. *J. Cell Biol.* **164**, 769–779, https://doi.org/10.1083/jcb.200307137
15 Sahin, U., Weskamp, G., Zheng, Y., Chesneau, V., Horiuchi, K. and Blobel, C.P. (2006) A sensitive method to monitor ectodomain shedding of ligands of the epidermal growth factor receptor. In *Methods in molecular biology. Methods in Molecular Biology* (Patel, T.B. and Bertics, P.J., eds), vol. 327, pp. 99–113, Humana Press, Clifton
16 Sanchez-Soria, P. and Camenisch, T.D. (2010) ErbB signaling in cardiac development and disease. *Semin. Cell Dev. Biol.* **21**, 929–935, https://doi.org/10.1016/j.semcdb.2010.09.011
17 Iwamoto, R. and Mekada, E. (2006) ErbB and HB-EGF signaling in heart development and function. *Cell Struct. Funct.* **31**, 1–14, https://doi.org/10.1247/csf.31.1
18 Jackson, L.F., Qiu, T.H., Sunnarborg, S.W., Chang, A., Zhang, C., Patterson, C. et al. (2003) Defective valvulogenesis in HB-EGF and TACE-null mice is associated with aberrant BMP signaling. *EMBO J.* **22**, 2704–2716, https://doi.org/10.1093/emboj/cdg264
19 Hassemer, E.L., Le Gall, S.M., Liegel, R., McNally, M., Chang, B., Zeiss, C.J. et al. (2010) The waved with open eyelids (woe) locus is a hypomorphic mouse mutation in Adam17. *Genetics* **185**, 245–255, https://doi.org/10.1534/genetics.109.113167
20 Horiuchi, K., Zhou, H.M., Kelly, K., Manova, K. and Blobel, C.P. (2005) Evaluation of the contributions of ADAMs 9, 12, 15, 17, and 19 to heart development and ectodomain shedding of neuregulins beta1 and beta2. *Dev. Biol.* **283**, 459–471, https://doi.org/10.1016/j.ydbio.2005.05.004
21 Shi, W., Chen, H., Sun, J., Buckley, S., Zhao, J., Anderson, K.D. et al. (2003) TACE is required for fetal murine cardiac development and modeling. *Dev. Biol.* **261**, 371–380, https://doi.org/10.1016/S0012-1606(03)00315-4
22 Hartmann, D., de Strooper, B., Serneels, L., Craessaerts, K., Herreman, A., Annaert, W. et al. (2002) The disintegrin/metalloprotease ADAM 10 is essential for Notch signalling but not for alpha-secretase activity in fibroblasts. *Hum. Mol. Genet.* **11**, 2615–2624, https://doi.org/10.1093/hmg/11.21.2615
23 Doyle, M.J., Lohr, J.L., Chapman, C.S., Koyano-Nakagawa, N., Garry, M.G. and Garry, D.J. (2015) Human induced pluripotent stem cell-derived cardiomyocytes as a model for heart development and congenital heart disease. *Stem Cell Rev.* **11**, 710–727, https://doi.org/10.1007/s12015-015-9596-6
24 Mital, S. (2016) Human Pluripotent Stem Cells to Model Congenital Heart Disease. In *Etiology and Morphogenesis of Congenital Heart Disease: From Gene Function and Cellular Interaction to Morphology* (Nakanishi, T., Markwald, R.R., Baldwin, H.S., Keller, B.B., Srivastava, D. and Yamagishi, H., eds), pp. 321–327, Springer, Tokyo
25 Botto, L.D., Lin, A.E., Riehle-Colarusso, T., Malik, S. and Correa, A. (2007) Seeking causes: classifying and evaluating congenital heart defects in etiologic studies. *Birth Defects Res. Part A, Clin. Mol. Teratol.* **79**, 714–727, https://doi.org/10.1002/bdra.20403

26 Xie, Y., Wang, D., Lan, F., Wei, G., Ni, T., Chai, R. et al. (2017) An episomal vector-based CRISPR/Cas9 system for highly efficient gene knockout in human pluripotent stem cells. *Sci. Rep.* **7**, 2320, https://doi.org/10.1038/s41598-017-02456-y
27 Lian, X., Hsiao, C., Wilson, G., Zhu, K., Hazeltine, L.B., Azarin, S.M. et al. (2012) Robust cardiomyocyte differentiation from human pluripotent stem cells via temporal modulation of canonical Wnt signaling. *Proc. Natl. Acad. Sci. U.S.A.* **109**, E1848–E1857, https://doi.org/10.1073/pnas.1200250109
28 Kim, D., Langmead, B. and Salzberg, S.L. (2015) HISAT: a fast spliced aligner with low memory requirements. *Nat. Methods* **12**, 357–360, https://doi.org/10.1038/nmeth.3317
29 Pertea, M., Pertea, G.M., Antonescu, C.M., Chang, T.C., Mendell, J.T. and Salzberg, S.L. (2015) StringTie enables improved reconstruction of a transcriptome from RNA-seq reads. *Nat. Biotechnol.* **33**, 290–295, https://doi.org/10.1038/nbt.3122
30 Pertea, M., Kim, D., Pertea, G.M., Leek, J.T. and Salzberg, S.L. (2016) Transcript-level expression analysis of RNA-seq experiments with HISAT, StringTie and Ballgown. *Nat. Protoc.* **11**, 1650–1667, https://doi.org/10.1038/nprot.2016.095
31 Robinson, M.D., McCarthy, D.J. and Smyth, G.K. (2010) edgeR: a Bioconductor package for differential expression analysis of digital gene expression data. *Bioinformatics* **26**, 139–140, https://doi.org/10.1093/bioinformatics/btp616
32 Mortazavi, A., Williams, B.A., McCue, K., Schaeffer, L. and Wold, B. (2008) Mapping and quantifying mammalian transcriptomes by RNA-Seq. *Nat. Methods* **5**, 621–628, https://doi.org/10.1038/nmeth.1226
33 Benjamini, Y., Drai, D., Elmer, G., Kafkafi, N. and Golani, I. (2001) Controlling the false discovery rate in behavior genetics research. *Behav. Brain Res.* **125**, 279–284, https://doi.org/10.1016/S0166-4328(01)00297-2
34 Liu, B., Ma, A., Zhang, F., Wang, Y., Li, Z., Li, Q. et al. (2016) MAZ mediates the cross-talk between CT-1 and NOTCH1 signaling during gliogenesis. *Sci. Rep.* **6**, 21534, https://doi.org/10.1038/srep21534
35 Lek, M., Karczewski, K.J., Minikel, E.V., Samocha, K.E., Banks, E., Fennell, T. et al. (2016) Analysis of protein-coding genetic variation in 60,706 humans. *Nature* **536**, 285–291, https://doi.org/10.1038/nature19057
36 Thomas, P.D. and Kejariwal, A. (2004) Coding single-nucleotide polymorphisms associated with complex vs. Mendelian disease: evolutionary evidence for differences in molecular effects. *Proc. Natl. Acad. Sci. U.S.A.* **101**, 15398–15403, https://doi.org/10.1073/pnas.0404380101
37 Schork, A.J., Thompson, W.K., Pham, P., Torkamani, A., Roddey, J.C., Sullivan, P.F. et al. (2013) All SNPs are not created equal: genome-wide association studies reveal a consistent pattern of enrichment among functionally annotated SNPs. *PLoS Genet.* **9**, e1003449, https://doi.org/10.1371/journal.pgen.1003449
38 Slaymaker, I.M., Gao, L., Zetsche, B., Scott, D.A., Yan, W.X. and Zhang, F. (2016) Rationally engineered Cas9 nucleases with improved specificity. *Science* **351**, 84–88, https://doi.org/10.1126/science.aad5227
39 Deschepper, C.F., Masciotra, S., Zahabi, A., Boutin-Ganache, I., Picard, S. and Reudelhuber, T.L. (2001) Functional alterations of the Nppa promoter are linked to cardiac ventricular hypertrophy in WKY/WKHA rat crosses. *Circ. Res.* **88**, 223–228, https://doi.org/10.1161/01.RES.88.2.223
40 Zaidi, S., Choi, M., Wakimoto, H., Ma, L., Jiang, J., Overton, J.D. et al. (2013) De novo mutations in histone-modifying genes in congenital heart disease. *Nature* **498**, 220–223, https://doi.org/10.1038/nature12141
41 Homsy, J., Zaidi, S., Shen, Y., Ware, J.S., Samocha, K.E., Karczewski, K.J. et al. (2015) De novo mutations in congenital heart disease with neurodevelopmental and other congenital anomalies. *Science* **350**, 1262–1266, https://doi.org/10.1126/science.aac9396
42 Sifrim, A., Hitz, M.P., Wilsdon, A., Breckpot, J., Turki, S.H., Thienpont, B. et al. (2016) Distinct genetic architectures for syndromic and nonsyndromic congenital heart defects identified by exome sequencing. *Nat. Genet.* **48**, 1060–1065, https://doi.org/10.1038/ng.3627
43 Jin, S.C., Homsy, J., Zaidi, S., Lu, Q., Morton, S., DePalma, S.R. et al. (2017) Contribution of rare inherited and de novo variants in 2,871 congenital heart disease probands. *Nat. Genet.* **49**, 1593–1601, https://doi.org/10.1038/ng.3970
44 Manolio, T.A., Collins, F.S., Cox, N.J., Goldstein, D.B., Hindorff, L.A., Hunter, D.J. et al. (2009) Finding the missing heritability of complex diseases. *Nature* **461**, 747–753, https://doi.org/10.1038/nature08494
45 Valente, A.M., Gauvreau, K., Assenza, G.E., Babu-Narayan, S.V., Schreier, J., Gatzoulis, M.A. et al. (2014) Contemporary predictors of death and sustained ventricular tachycardia in patients with repaired tetralogy of Fallot enrolled in the INDICATOR cohort. *Heart* **100**, 247–253, https://doi.org/10.1136/heartjnl-2013-304958
46 Gordon, W.R., Roy, M., Vardar-Ulu, D., Garfinkel, M., Mansour, M.R., Aster, J.C. et al. (2009) Structure of the Notch1-negative regulatory region: implications for normal activation and pathogenic signaling in T-ALL. *Blood* **113**, 4381–4390, https://doi.org/10.1182/blood-2008-08-174748
47 Gordon, W.R., Vardar-Ulu, D., L'Heureux, S., Ashworth, T., Malecki, M.J., Sanchez-Irizarry, C. et al. (2009) Effects of S1 cleavage on the structure, surface export, and signaling activity of human Notch1 and Notch2. *PLoS ONE* **4**, e6613, https://doi.org/10.1371/journal.pone.0006613
48 Huppert, S.S., Le, A., Schroeter, E.H., Mumm, J.S., Saxena, M.T., Milner, L.A. et al. (2000) Embryonic lethality in mice homozygous for a processing-deficient allele of Notch1. *Nature* **405**, 966–970, https://doi.org/10.1038/35016111
49 Fischer, A., Schumacher, N., Maier, M., Sendtner, M. and Gessler, M. (2004) The Notch target genes Hey1 and Hey2 are required for embryonic vascular development. *Genes Dev.* **18**, 901–911, https://doi.org/10.1101/gad.291004
50 Peschon, J.J., Slack, J.L., Reddy, P., Stocking, K.L., Sunnarborg, S.W., Lee, D.C. et al. (1998) An essential role for ectodomain shedding in mammalian development. *Science* **282**, 1281–1284, https://doi.org/10.1126/science.282.5392.1281
51 Zhao, J., Chen, H., Peschon, J.J., Shi, W., Zhang, Y., Frank, S.J. et al. (2001) Pulmonary hypoplasia in mice lacking tumor necrosis factor-alpha converting enzyme indicates an indispensable role for cell surface protein shedding during embryonic lung branching morphogenesis. *Dev. Biol.* **232**, 204–218, https://doi.org/10.1006/dbio.2001.0176
52 Blaydon, D.C., Biancheri, P., Di, W.L., Plagnol, V., Cabral, R.M., Brooke, M.A. et al. (2011) Inflammatory skin and bowel disease linked to ADAM17 deletion. *N. Engl. J. Med.* **365**, 1502–1508, https://doi.org/10.1056/NEJMoa1100721
53 Maretzky, T., McIlwain, D.R., Issuree, P.D., Li, X., Malapeira, J., Amin, S. et al. (2013) iRhom2 controls the substrate selectivity of stimulated ADAM17-dependent ectodomain shedding. *Proc. Natl. Acad. Sci. U.S.A.* **110**, 11433–11438, https://doi.org/10.1073/pnas.1302553110